2024 IEEE International Conference on Robotics and Automation (ICRA 2024)
May 13-17, 2024. Yokohama, Japan

Design and Analysis of Soft Hybrid-Driven Manipulator with Variable Stiffness and Multiple Motion Patterns

Xin Fu[1,2,3], Daohui Zhang[1,2*], Liyan Mo[1,2,3], Kai Li[1,2,3] and Xingang Zhao[1,2]

Abstract— **Soft manipulators offer the advantages of safety and adaptability. However, due to insufficient stiffness and single motion mode limitations, existing soft manipulators usually exhibit low load capacity and small working space. To address this problem, we propose a novel soft hybrid-driven manipulator with continuous stiffness control capability and multiple motion patterns (omnidirectional bending and extension). Furthermore, we develop kinematic and stiffness models based on the constant curvature assumption. The soft robot consists of a soft bellows actuator and inextensible rigid skeletons, which exhibit a high extension ratio and low drive pressure. With the antagonistic actuation of tendon-pulling and air-pushing, the robot can achieve independent control over stiffness and position in three-dimensional space. The performance associated with the designed soft hybrid-driven manipulator is experimentally verified. The robot can achieve an elongation of 198% and a maximum bending angle of up to 240°. The robot can also increase stiffness by increasing internal air pressure to resist deformation caused by external loads. Additionally, tracking experiments with various trajectories in space verify the accuracy of the kinematic model, which indicates that the soft manipulator can stabilize motion within a broad workspace.**

I. Introduction

Soft robots, which are typically constructed from materials with a low Young's modulus, have considerable potential in various domains, such as human-robot interaction [1], [2], underwater operations [3], compliant grasping [4], and locomotion [5], due to their compliance, deformability, and safety. These soft robots can be effectively controlled through various actuation methods, including tendons [6], elastic push-pull rods [7], fluids [8], shape-memory alloys [9], and dielectric elastomers [10], which enable multiple deformation modes. However, soft robots still exhibit significant limitations in terms of flexible deformation and load capacity.

Several approaches have been investigated to achieve a compromise between two conflicting factors: extensive deformation characteristics and load characteristics. Commonly employed approaches include single-drive techniques, as well as variable stiffness designs such as magnetorheological (MR) materials [11], low-melting-point alloys [12], thermoplastic polymers [13], particle blocking[14], layer blocking [15], and others. These methodologies possess the capacity to significantly modify the stiffness, albeit at the expense of complicating the system's structure and diminishing the robot's maneuverability. Additionally, they typically do not offer the capability for continuous stiffness adjustment. By utilizing a variable length strain-limiting layer composed of hybrid fiber [16] or cable locking system [17], it is possible to be able to achieve multiple motion modes and continuous stiffness control. Nevertheless, the passive control of the strain-limiting layer has implications for motion control performance.

In nature, invertebrates like octopuses exhibit a diverse range of locomotor behaviors, including elongation, bending, and twisting, which are achieved through coordinating antagonistic muscle groups [18], [19]. Additionally, they can modulate stiffness over a wide range to ensure manipulation stability. Antagonistic actuation presents a potential methodology for advancing the design of soft robots characterized by flexible deformation and variable stiffness. The implementation of antagonistic actuation in robots can be realized by passive antagonism. Thien-Dang Nguyen et al. [20], [21] developed a novel continuum manipulator with a permanent magnet spacer disk skeleton that utilizes tendon and magnetic repulsive forces to achieve multimodal robot motion. However, due to passive antagonism, the magnetic force decreases rapidly with the extension of each part, reducing its kinematic performance. The active antagonism form, which can adjust the magnitude of the antagonistic stress, possesses broader application prospects. The European Union-funded STIFF-FLOP program developed a medical soft manipulator that is propelled uniformly by three air chambers and three variable stiffness functional chambers [22], [23]. Xifeng Gao et al. proposed a pneumatic lightweight soft continuum manipulator with flexor and extensor muscles which achieves decoupled control of stiffness and position by regulating the air pressure within the extensor and flexor muscles [24]. However, most of these designs employ chambers that consist of a single cylindrical structure, resulting in restricted telescoping capabilities. This diminishes the flexibility and workspace of soft robots and makes it difficult for robots to perform tasks such as spatial spiral trajectory tracking. Therefore, soft manipulators with flexible workspace and variable bending stiffness still need further research.

The main contribution of this study is the design of a novel soft hybrid-driven manipulator for multimodal motion and continuous stiffness control. The design of the proposed robot incorporates a silicone bellow actuator and external rigid skeletons as the core structure of the soft robot. Three tendons

This work was supported in part by the National Natural Science Foundation of China (92048302, 62273336, 62203430, U20A20197, U22A2067), the National Key Research and Development Program of China (2023YFB4704700, 2023YFB4704702, 2022YFF1202500, 2022YFF1202502), the Liaoning Revitalization Talents Program (XLYC1908030), and China Postdoctoral Science Foundation funded project (2022M723312).

1. State Key Laboratory of Robotics, Shenyang Institute of Automation, Chinese Academy of Sciences, Shenyang, China.
2. Institutes for Robotics and Intelligent Manufacturing, Chinese Academy of Sciences, Shenyang, China.
3. University of Chinese Academy of Sciences, Beijing, China.
* Contact: Daohui Zhang (zhangdaohui@sia.cn)

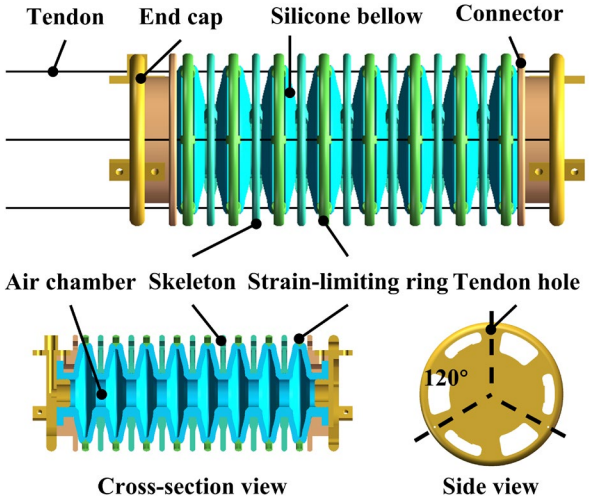

Fig. 1. The design schematic of the soft hybrid-driven manipulator.

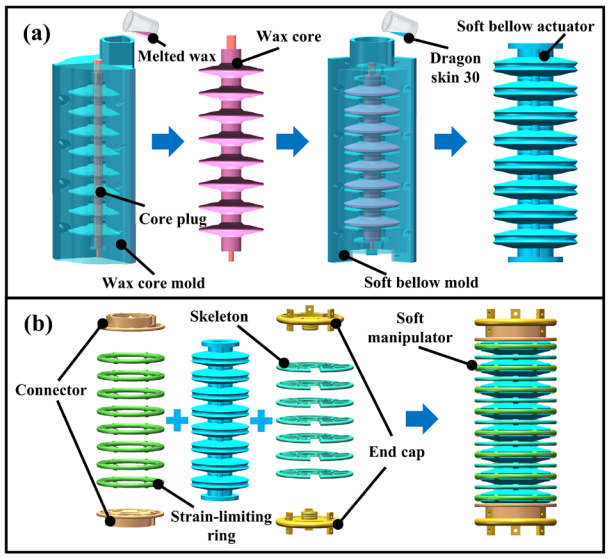

Fig. 2. The fabrication process and assembly of the soft hybrid-driven manipulator. (a) The casting of silicone bellows cavities using the lost wax method. (b) Assemble the silicone bellows cavity with the skeletons, strain-limiting rings, end caps, and connectors.

are strategically placed along the outer circumference of the skeletons. The flexible bellows structure facilitates a wide range of telescopic motion with minimal input inflation pressure, while the tendons enable omnidirectional bending. Moreover, the high actuation accuracy of the tendons allows for precise movements, enabling accurate tracking of various trajectories in space. The robot also utilizes the antagonistic effects of hybrid actuation of tendon-driven and pneumatic actuators to achieve variable stiffness.

The remaining sections of the paper are structured as follows. Section II provides a detailed explanation of the concept and fabrication process of the soft hybrid-driven manipulator. In Section III, models for kinematic and stiffness adjustment based on constant curvature are developed. The experimental processes and results are outlined in Section IV. Finally, Section V serves as the conclusion of the paper.

II. Manipulator and Fabrication

A. Robot Design

To address the requirement for flexible and precise operation of soft robots, we have developed a soft hybrid-driven manipulator with continuous stiffness control capability and multiple motion patterns (omnidirectional bending and extension). The soft manipulator exhibited dimensions of 160mm in length and 62mm in diameter. As shown in Fig. 1, the module comprises a silicone bellow actuator, 3D-printed rigid strain-limiting rings, support skeletons, connectors, and end caps. The rigid constraint rings and skeletons feature tendon-guiding holes, which are evenly distributed at 120° intervals along the circumference. A flexible soft bellow actuator made by Dragon Skin 30 can be actuated by air. In comparison to conventional fiber-reinforced silicone structures, the circular symmetric bellow structure provides rapid actuation capabilities and can produce significant elongation with minimal pressure. Moreover, strain-limiting rings are installed at the outer diameter to restrict radial expansion, while rigid skeletons are installed at the inner circumferential grooves to enhance the structural stiffness. Three tendons traverse the guiding rings on the rigid structure, with one end affixed to the end cap and the other end secured to the winding pulley. By employing the antagonistic driving principle, the soft manipulator can achieve various motion modes, including bending, elongation, and controllable stiffness.

B. Fabrication Process

One of the challenges in the fabrication process of the soft bellow structure lies in its intricate internal geometry. In our work, we employ the lost wax method for the fabrication of the soft bellow actuator, wherein the air chamber is constructed using Dragon Skin 30. The specific manufacturing process is illustrated in Fig. 2.

First, molds for wax core making are created through 3-D printing technology. The melted wax was then poured into the assembled mold and a rigid core plug was inserted to facilitate subsequent fixation. Once the paraffin wax was cooled down, the wax core was extracted and processed to achieve a smooth and burr-free surface. And then, the wax core was assembled with the 3D printed rigid outer molds and silicone release (Universal Mold Release from Smooth-on, Inc) was sprayed to all surfaces to facilitate easy removal of the soft bellow actuator. Following this, silicone rubber (Dragon Skin 30) was injected into the molds. After the silicone gel was cured, the bellows with wax core were removed and heated to 70°C in an oven to melt away the wax cores. The complete soft bellow actuator can be seen in Fig. 2(a).

Finally, external rigid strain-limiting rings were affixed to the corrugated tube using silicone adhesive (Sil-Poxy), and rigid skeletons were installed at the grooves of the bellows. Both parts of the manipulator were fitted with end caps and connectors, as Fig. 2(b) shows. So far, the soft robot was fabricated.

C. Prototype System Description

The complete prototype system is shown in Fig. 3. The tendons are secured on the winding wheel, and the computer

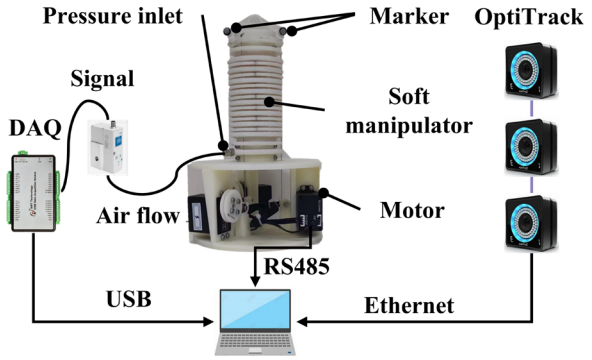

Fig. 3. Overview of the soft manipulator experiments setup.

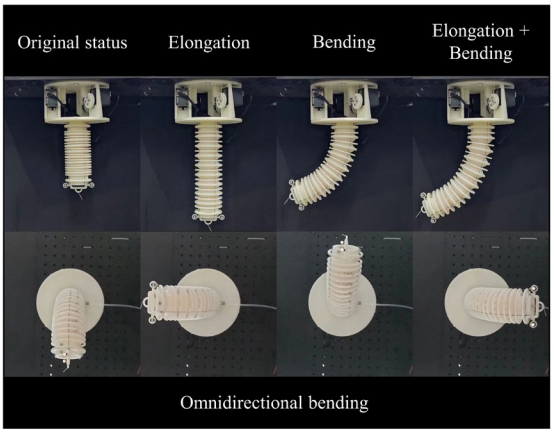

Fig. 4. Multiple motion patterns of the soft hybrid-driven manipulator.

adjusts the length of the tendons by manipulating the angle of three servo motors (FEETECH SM29BL) through the RS485 bus. A DAQ (ART USB3133A) is used to receive commands from the computer to regulate the output air pressure of the pneumatic regulator. Additionally, two reflective markers are installed at the tip to measure the end position of the soft manipulator during experimental trials utilizing three OptiTrack cameras.

D. Multiple Motion Patterns and Variable Stiffness

The soft hybrid-driven manipulator we designed can produce multiple motion patterns (see Fig. 4) under the synchronized drive of tendons and air pressure. When all tendons are fully released, the tendons can move freely with the air chamber and thus can be driven by air pressure as a linear actuator. When one of the tendons is in a locked state, the actuator will bend in the corresponding direction due to air pressure. By independently controlling the lengths of the three tendons, the soft robot achieves omnidirectional bending motion. Moreover, the lengths of tendons dictate the maximum extension of the silicone bellow actuator, allowing for the adjustment of internal stress by varying pressure levels, consequently altering the stiffness of the air cavity.

III. Analytical Modeling of the Manipulator

In this section, we establish the kinematic model of the soft manipulator based on the constant curvature [25] assumption and analyze the principle that the manipulator can

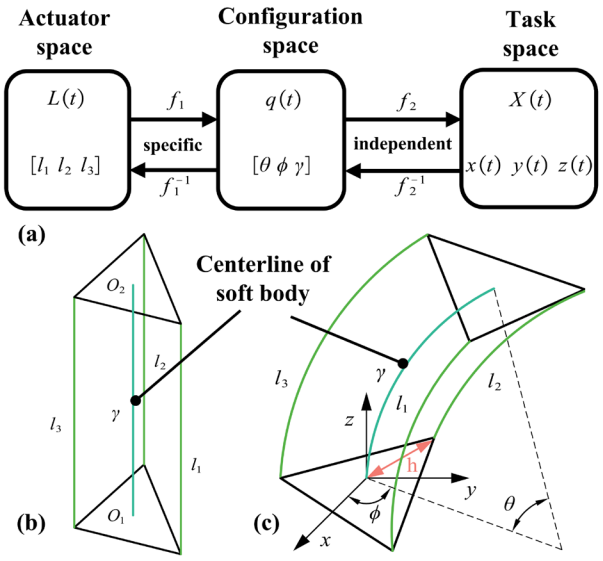

Fig. 5. Kinematics of the soft manipulator. (a) Kinematic mapping based on the constant curvature assumption for continuum robots. (b) The initial state of a soft manipulator. (c) Structure and arc parameters of a continuum module.

independently control its stiffness and position by adjusting the internal air pressure of the bellows.

A. Forward Kinematics

As shown in the Fig. 5(a), the kinematic model of the soft robot can be categorized into specific and independent mappings. The actuator space consists of cable lengths (l_1, l_2, l_3), while the configuration space consists of three arc-shaped parameters (θ, ϕ, γ) that describe the geometrical shape of the soft manipulator. The task space consists of the position (x, y, z) of the soft manipulator's end effector.

The forward kinematics describes the transformation from the actuator space to the task space. The initial simplified model of the soft manipulator is shown in Fig. 5(b), where the deformable shape of the soft robot is quantified by points along the central line. A coordinate system is then established to describe the geometrical shape of the soft manipulator, as shown in Fig. 5(c). The coordinate system origin is fixed at the center of the soft manipulator base. Additionally, arc-shaped parameters in the configuration space, including length (γ), rotation angle (ϕ), and bending angle (θ), are labeled in Fig. 5(c). The distance h between the center point O_1 and the tendon guide hole is 31 mm. The mapping relationship from the actuator space to the configuration space can be established as shown as follows:

$$\begin{aligned} \theta &= \frac{(l_1 + l_2 + l_3)}{3} \\ \phi &= \operatorname{atan2}\left(\sqrt{3}(l_1 + l_2 - 2l_3), 3(l_2 - l_3)\right) \\ \gamma &= \frac{2\sqrt{l_1^2 + l_2^2 + l_3^2 - l_1 l_2 - l_1 l_3 - l_2 l_3}}{3h} \end{aligned} \tag{1}$$

The mapping from the configuration space to the task space of the soft manipulator can be easily described using homogeneous matrices:

$$T=\begin{bmatrix} R_{z,\phi} & 0 \\ 0 & 1 \end{bmatrix}\begin{bmatrix} R_{y,\theta} & p \\ 0 & 1 \end{bmatrix}\begin{bmatrix} R_{x,-\phi} & 0 \\ 0 & 1 \end{bmatrix}=\begin{bmatrix} R & p \\ 0 & 1 \end{bmatrix}$$

$$=\begin{bmatrix} 1+c^2\phi(c\theta-1) & s\phi c\phi(c\theta-1) & c\phi s\theta & \dfrac{\gamma c\phi(1-c\theta)}{\theta} \\ c\phi s\theta(c\theta-1) & 1+s^2\phi(c\theta-1) & s\phi s\theta & \dfrac{\gamma s\phi(1-c\theta)}{\theta} \\ -c\phi s\theta & -s\phi s\theta & c\theta & \dfrac{\gamma s\theta}{\theta} \\ 0 & 0 & 0 & 1 \end{bmatrix} \tag{2}$$

where $c\theta=\cos\theta$, and $s\theta=\sin\theta$, the same to ϕ.

The forward kinematics of the soft manipulator consists of (1) and (2), serving as the foundation for the subsequent establishment of the inverse kinematics.

B. Inverse Kinematics

Inverse kinematics is a crucial aspect of trajectory planning and task completion in the field of soft manipulators, thus highlighting its significance. It involves determining the necessary lengths of tendons and the module to control the movement of the soft manipulator, based on the provided end position information. This enables the conversion from task space to actuator space. When the desired end position $(x,\ y,\ z)$ is given, the configuration space variables can be computed using the following equation:

$$\begin{aligned} \theta &= \operatorname{atan2}\left(2z\sqrt{(x^2+y^2)}, z^2-(x^2+y^2)\right) \\ \phi &= \operatorname{atan2}(y,x) \\ \gamma &= z\theta/\sin\theta \end{aligned} \tag{3}$$

After receiving the assignment of configuration space transformation, it becomes imperative to compute the length of the tendons in the actuator space. By assuming that the cross-section of each segment remains constant throughout the deformation of the soft manipulator, the length of each tendon can be expressed as follow:

$$l_i=\theta\left(\gamma-h\cos\left(\frac{\pi}{2}+\frac{2\pi(i-1)}{3}-\phi\right)\right) \tag{4}$$

where $i=1,\ 2,\ 3$ represents the length of three driving tendons.

Thus, we acquired the mapping relationship between the task space coordinates and the drive space $(l_1,\ l_2,\ l_3)$ coordinates, which serves as the basis for subsequent trajectory tracking.

C. Stiffness Model

The core of stiffness variation is based on the regulation of internal pressure in the bellows. The mechanism of stiffness variation is analyzed based on the assumption that the deformation curve of the soft robot in the case of end force can still be approximated as a constant curvature. The definition of stiffness is as follows:

$$K=\frac{F}{\Delta x} \tag{5}$$

The force F represents the vertically downward force applied at the end of the soft manipulator. As is shown in Fig. 6(a), it can be observed that the bending angle changes from θ to θ' as the module transitions from its free state to the loaded state. The bending deformation cross-section of the module is shown in Fig. 6(b). Additionally, due to the inextensibility of the line, the length of the axis of the module remains constant. The driving air pressure is P, which is kept constant. By disregarding the effect of gravity and the deformation of the silicone gel before and after loading, we can utilize the principle of virtual work to derive the following equation:

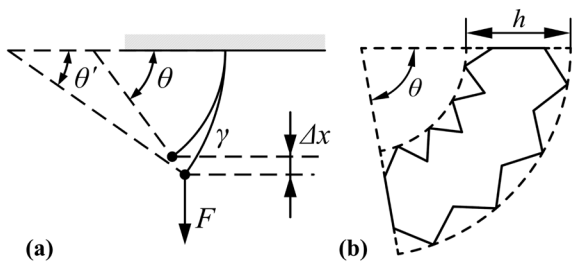

Fig. 6. Model deformation analysis by external force. (a) Configuration of the soft manipulator under external load. (b) Module bending deformation cross-section.

$$P\cdot\Delta V=\frac{1}{2}F\Delta x \tag{6}$$

where ΔV is the amount of change in volume inside the bellows.

The actuator volume V is given by:

$$V=2\gamma\int_{-h/2}^{h/2}\sqrt{d^2-x^2}\,dx\cdot\varepsilon \tag{7}$$

where h is the diameter of the bellows, ε is the correction term introduced for the cross-sectional area of the fixed actuator, representing a nonlinear mapping related to the posture of the soft manipulator, as is shown in Fig. 6(b). Considering the complexity of establishing the mapping relationship based on the silicone gel constitutive model, this aspect will be studied in future work.

Substitute (5)(7) into (6), we get:

$$K=4PAC\gamma \tag{8}$$

where $C=(\varepsilon_1-\varepsilon_2)/(l\sin\theta'/\theta'-l\sin\theta/\theta)^2$ is a constant, $A=\int_{-h/2}^{h/2}\sqrt{h^2-x^2}\,dx$.

In the stiffness model, the stiffness of the soft manipulator is determined by the internal pressure within the air chamber. Specifically, at a given position, the pressure P can be actively adjusted to respond to changes in external forces. This lays the foundation for future active regulation of stiffness, which is not described in detail in this paper.

IV. Experiments and Results

This section presents an experimental study of the soft robot, which includes tests for elongation, bending, and stiffness. Furthermore, closed-loop trajectory tracking experiments were conducted to test the kinematic model and verify the dynamic motion capabilities, for spiral and square paths, respectively.

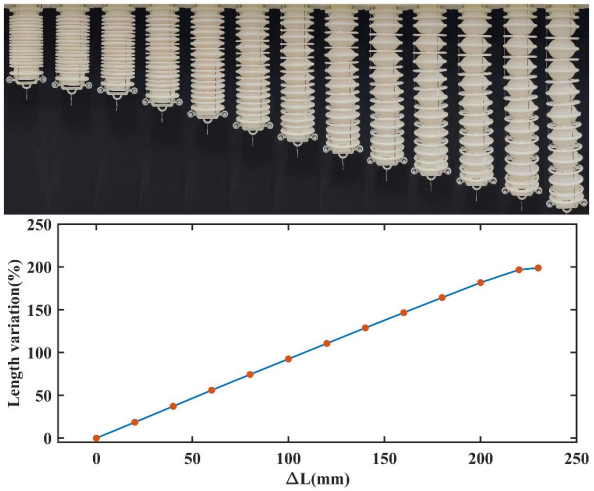

Fig. 7. The elongation of a soft hybrid-driven manipulator under the action of tendon pulling and pneumatic pushing with a fixed internal air pressure of 0.5 bar.

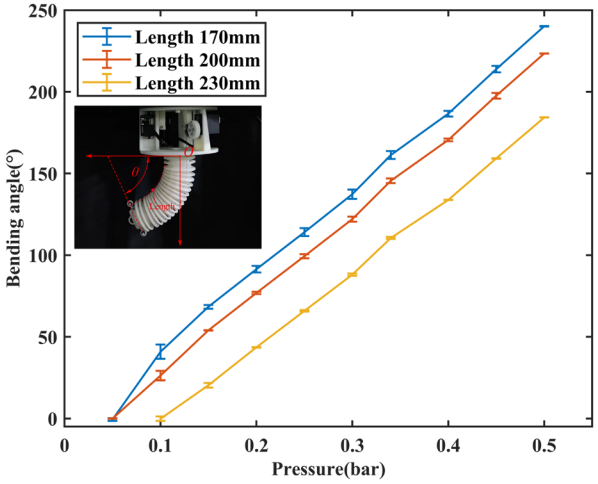

Fig. 8. The bending capacity of the soft manipulator at different lengths.

A. Motion Capacity

1) *Elongation:* The elongation movement of the module can be achieved by changing the length of the tendon after filling the internal chamber with a fixed air pressure, as tendons can only experience tensile force. For safety, the internal air pressure was maintained at 0.5 bar throughout the elongation experiments. Firstly, the module was contracted to its shortest position. Subsequently, three tendons were elongated at the same rate to achieve a pure axial elongation of the module. As shown in Fig. 7, the module elongated from 110mm to 328mm as the three tendons elongated. The maximum elongation rate is 198% compared to the initial length. Due to the high accuracy of the tendon actuation, the module length is highly linear concerning the length of the tendons. When the internal cavity length reaches a maximum value of 328 mm, thereafter, the module length no longer changes as the tendon length increases.

2) *Bending:* In the bending experiment, only one tendon is locked while the other two tendons remain relaxed. By increasing the pressure inside the air chamber, the module bends towards the immobilized tendon. Additionally, changing the length of the tendon allows for coupled motion of elongation and bending. Three sets of experiments were conducted, with the tendon being actuated to elongate to 170 mm, 200 mm, and 230 mm, respectively. In each set of experiments, the tendon was initially prompted to attain the desired length, followed by incremental inflation of the pressure from 0 bar to 0.5 bar in 0.05 bar increments. The spatial position of the endpoint mark points of the module was measured to calculate the bending angle. According to the experimental results in Fig. 8, it can be observed that the bending angle of the module decreases as the locked tendon length increases at a constant driving pressure. This phenomenon is attributed to the linear relationship between chamber length and air pressure, wherein an elongated tendon necessitates a greater chamber length to achieve a consistent bending angle. Consequently, the maximum bending angle of the module decreases with increasing length of the locking tendon at a pressure of 0.5 bar. Specifically, at a length of 170mm, the module can achieve a bending angle of 240°, which indicates its flexible range of motion.

B. Variable Stiffness

With the antagonistic actuation of tendon-pulling and air-pushing, the module can achieve independent control over stiffness and position in three-dimensional space. To evaluate the effectiveness of active stiffness control in the vertical direction of the module, two sets of experiments were conducted to verify the effects of different bending angles and module lengths on the stiffness, respectively. The stiffness in each set of experiments was determined through the measurement of height change resulting from the application of a 500 g weight at the module's end, as illustrated in Fig. 9(a). This calculation was then carried out using (5).

In the first set of tests, the module was bent at a fixed angle of 60°. The internal air chamber of the module was first inflated to maintain the pressure at 1.5 bar, then three tendons were activated to extend the control module to 140 mm, 170 mm, and 200 mm, and the position of the end of the module was recorded at this point, then a 500g weight was fixed to the end of the module. The internal pressure of the control chamber was then gradually reduced from 1.5 bar to 0.5 bar in 0.1 bar increments while the end position offset was recorded. In the second set of tests, the initial length of the module was kept at 170 mm and bent to 30°, 60°, and 90°. The rest of the testing process is the same as the first group.

As shown in Fig. 9(b) and Fig. 9(c), the relationship between air pressure and stiffness of the soft robot under different configurations is displayed. At a given position, the stiffness increases proportionally with the increase in pressure. This trend aligns with the analytical model (8), and the linear regression model derived from experimental data effectively elucidates the connection between air pressure and stiffness. At 0.5 bar air pressure, the bending stiffness can reach a minimum of 0.22 N/mm, which gives it natural softness and safe interaction; at 1.5 bar air pressure, the bending stiffness can reach a maximum of 2.39 N/mm, which provides a higher load-bearing capacity. With the module length of 170 mm and a bending angle of 60°, the stiffness of the module is 0.32 N/mm at an internal air pressure of 0.5 bar.

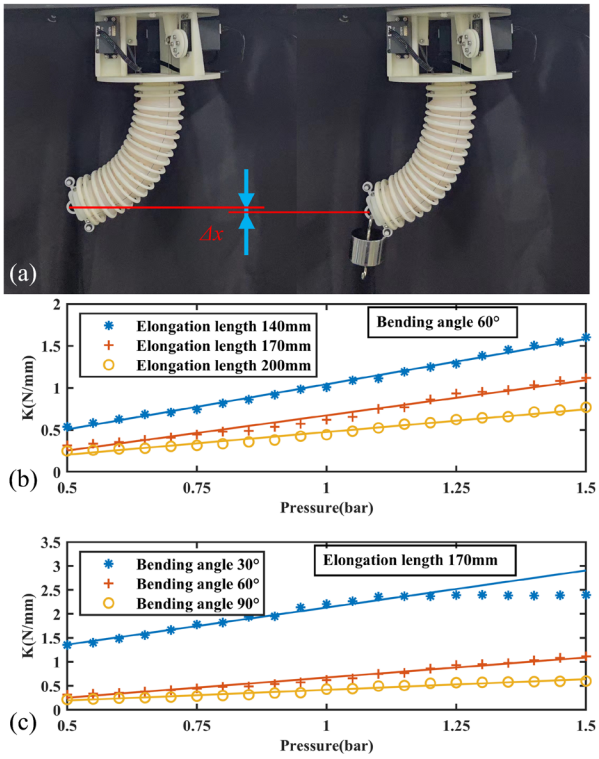

Fig. 9. The bending stiffness characterization of the soft manipulator. (a) Schematic diagram of stiffness test. (b) When the same angle of bending is applied, different elongations correspond to changes in stiffness. (c) Variations in stiffness with different angles of bending at equal length extension.

When the air pressure is increased to 1.5 bar, the bending stiffness of the robot increases to 1.12 N/mm, which is approximately 3.5 times the initial stiffness.

The rate of change in the bending stiffness of the robot increases gradually with the deformation of the silicone material as the air pressure increases. This relationship will be analyzed extensively in the future, using the hyper elasticity intrinsic model of silicone. Based on the comparative findings from the two sets of experiments, it can be observed that the stiffness of the soft robot decreases as the bending angle and extension length increase, all while maintaining the same air pressure. This decline in stiffness can be attributed to the augmented moment generated by the weights placed on the base. Meanwhile, at a bending angle of 30°, the change in stiffness is not significant at high air pressure. This is because the weights produce less bending moment at the base and the height change at the end position is relatively small. In conclusion, increasing the air pressure can enhance the stiffness and improve the practical operation of the robot.

C. Tip Trajectory Tracking

To assess the precision of the kinematic model and the controllable generalized motion capabilities of the robot, two distinct trajectories were employed to analyze its tracking performance. Meanwhile, one of the trajectories selected was a spatial spiral, considering the extensive workspace facilitated by the extendable properties of the soft robot. Firstly, we discretize a continuous trajectory into a series of discrete points in space. With a predetermined inflation

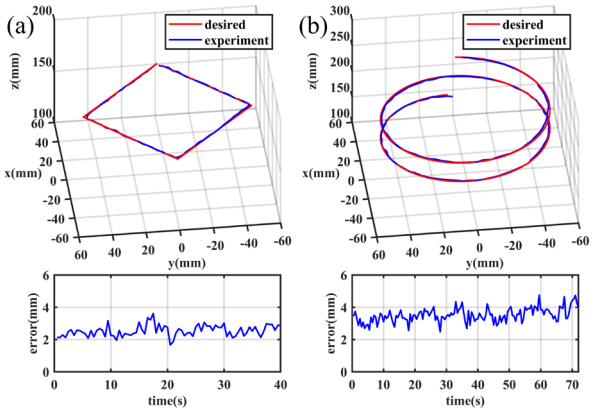

Fig. 10. The results of the path tracing task are presented for (a) a planar square and (b) a spatial spiral.

pressure of 1.2 bar, the soft manipulator is controlled to track the defined trajectory using the kinematic model. The real-time position of the end was recorded using a T265 tracking camera, and then the difference between the actual position and the target position was used to calculate the drive length of the tendon to meet the target position. Fig. 10 illustrates the results of tracking planar square and spatial spiral paths. The soft manipulator demonstrates good tracking performance under closed-loop control, with root-mean-square deviations of 2.48 mm and 3.51 mm respectively. However, the tracking error occasionally exhibits oscillations due to external interference and model errors, although it remains within a narrow range. This confirms the accuracy of the kinematic model and demonstrates the soft manipulator's ability to accurately track the reference trajectory. Tracking accuracy is affected by factors such as motion model errors and system lag.

V. Conclusion

This study proposed a novel hybrid-driven soft manipulator with variable stiffness and multiple motion patterns. The robot utilizes a bellow structure and skeletons, which results in a large telescopic deformation capability, and a low input pressure actuation. By utilizing the antagonistic interaction between tendons and pneumatic actuators, the motion and stiffness of the soft robot can be controlled simultaneously in 3D space. The robot can increase the original actuator length up to 198% and achieve substantial bending deformations, thereby expanding the workspace. In addition, the stiffness of the robot exhibits a linear correlation with the internal air pressure, resulting in a notable enhancement in load-bearing capacity. The soft robot proposed in this study effectively balances motion range, workspace, and stiffness adaptability, indicating promising prospects for practical applications.

In future work, adaptive control algorithms will be utilized to modulate the stiffness of soft robots by incorporating kinematic and stiffness models. This will enable the soft robot to dynamically modify their stiffness levels in response to varying task during interactions with unknown environments.

REFERENCES

[1] Z. Tang, P. Wang, W. Xin, and C. Laschi, "Learning-Based Approach for a Soft Assistive Robotic Arm to Achieve Simultaneous Position and Force Control," IEEE Robotics and Automation Letters, vol. 7, no. 3, pp. 8315–8322, Jul. 2022.

[2] H. K. Yap et al., "A Fully Fabric-Based Bidirectional Soft Robotic Glove for Assistance and Rehabilitation of Hand Impaired Patients," IEEE Robotics and Automation Letters, vol. 2, no. 3, pp. 1383–1390, Jul. 2017.

[3] Z. Gong et al., "A soft manipulator for efficient delicate grasping in shallow water: Modeling, control, and real-world experiments," The International Journal of Robotics Research, vol. 40, no. 1, pp. 449–469, Jan. 2021.

[4] S. Jain, S. Dontu, J. E. M. Teoh, and P. Valdivia Y Alvarado, "A Multimodal, Reconfigurable Workspace Soft Gripper for Advanced Grasping Tasks," Soft Robotics, Nov. 2022.

[5] Z. Wan et al., "Design, Analysis, and Real-Time Simulation of a 3D Soft Robotic Snake," Soft Robotics, vol. 10, no. 2, pp. 258–268, Apr. 2023.

[6] J. Lai, B. Lu, and H. K. Chu, "Variable-Stiffness Control of a Dual-Segment Soft Robot Using Depth Vision," IEEE/ASME Transactions on Mechatronics, vol. 27, no. 2, pp. 1034–1045, Apr. 2022.

[7] P. Wang, Z. Tang, W. Xin, Z. Xie, S. Guo, and C. Laschi, "Design and Experimental Characterization of a Push-Pull Flexible Rod-Driven Soft-Bodied Robot," IEEE Robotics and Automation Letters, vol. 7, no. 4, pp. 8933–8940, Oct. 2022.

[8] J. Davies et al., "Hydraulically Actuated Soft Tubular Gripper," in 2022 International Conference on Robotics and Automation (ICRA), May 2022, pp. 6144–6150.

[9] Z. AL-Rabia, M. Al-Ibadi, and A. Al-Ibadi, "Design and Implementation of a Multiple DoF Soft Robot Arm Using Exestensor Muscles," in 2022 9th International Conference on Electrical and Electronics Engineering (ICEEE), Mar. 2022, pp. 170–174.

[10] E. Hajiesmaili and D. R. Clarke, "Dielectric elastomer actuators," Journal of Applied Physics, vol. 129, no. 15, p. 151102, Apr. 2021.

[11] L. Huang, H. Hu, and Q. Ouyang, "Design and Feasibility Study of MRG–Based Variable Stiffness Soft Robot," Micromachines, vol. 13, no. 11, Art. no. 11, Nov. 2022.

[12] H. Wang, Z. Chen, and S. Zuo, "Flexible Manipulator with Low-Melting-Point Alloy Actuation and Variable Stiffness," Soft Robotics, vol. 9, no. 3, pp. 577–590, Jun. 2022.

[13] J. Yan, P. Shi, Z. Xu, and J. Zhao, "A Wide-Range Stiffness-Tunable Soft Actuator Inspired by Deep-Sea Glass Sponges," Soft Robotics, vol. 9, no. 3, pp. 625–637, Jun. 2022.

[14] Y. Wei et al., "A Novel, Variable Stiffness Robotic Gripper Based on Integrated Soft Actuating and Particle Jamming," Soft Robotics, vol. 3, no. 3, pp. 134–143, Sep. 2016.

[15] L.-J. Gai, J. Huang, and X. Zong, "Stiffness-Tunable Soft Bellows Actuators by Cross-Fiber Jamming Effect for Robust Grasping," IEEE/ASME Transactions on Mechatronics, pp. 1–11, 2023.

[16] R. Chellattoan and G. Lubineau, "A Stretchable Fiber with Tunable Stiffness for Programmable Shape Change of Soft Robots," Soft Robotics, Jan. 2022.

[17] Q. Xiong, X. Zhou, and C.-H. Yeow, "A Soft Pneumatic Actuator with Multiple Motion Patterns Based on Length-tuning Strain-limiting Layers," in 2023 IEEE International Conference on Soft Robotics (RoboSoft), Apr. 2023, pp. 1–6.

[18] M. Cianchetti, A. Arienti, M. Follador, B. Mazzolai, P. Dario, and C. Laschi, "Design concept and validation of a robotic arm inspired by the octopus," Materials Science and Engineering: C, vol. 31, no. 6, pp. 1230–1239, Aug. 2011.

[19] K. Althoefer, "Antagonistic actuation and stiffness control in soft inflatable robots," Nat Rev Mater, vol. 3, no. 6, Art. no. 6, Jun. 2018.

[20] T.-D. Nguyen and J. Burgner-Kahrs, "A tendon-driven continuum robot with extensible sections," in 2015 IEEE/RSJ International Conference on Intelligent Robots and Systems (IROS), Sep. 2015, pp. 2130–2135.

[21] E. Amanov, T.-D. Nguyen, and J. Burgner-Kahrs, "Tendon-driven continuum robots with extensible sections—A model-based evaluation of path-following motions," The International Journal of Robotics Research, vol. 40, no. 1, pp. 7–23, Jan. 2021.

[22] M. Cianchetti, T. Ranzani, G. Gerboni, I. De Falco, C. Laschi, and A. Menciassi, "STIFF-FLOP surgical manipulator: Mechanical design and experimental characterization of the single module," in 2013 IEEE/RSJ International Conference on Intelligent Robots and Systems, Nov. 2013, pp. 3576–3581.

[23] A. Shiva et al., "Tendon-Based Stiffening for a Pneumatically Actuated Soft Manipulator," IEEE Robotics and Automation Letters, vol. 1, no. 2, p. 6, 2016.

[24] X. Gao, X. Li, C. Zhao, L. Hao, and C. Xiang, "Variable stiffness structural design of a dual-segment continuum manipulator with independent stiffness and angular position," Robotics and Computer-Integrated Manufacturing, vol. 67, p. 102000, Feb. 2021.

[25] R. J. Webster and B. A. Jones, "Design and Kinematic Modeling of Constant Curvature Continuum Robots: A Review," The International Journal of Robotics Research, vol. 29, no. 13, pp. 1661–1683, Nov. 2010.